Quantum Electronics **36** (5) 408 – 414 (2006)

NONLINEAR OPTICAL PHENOMENA

PACS numbers: 42.62.Fi; 78.47.+p; 74.25.Gz; 78.20.Bh
DOI: 10.1070/QE2006v036n05ABEH013234

Features of the nonlinear response of high-temperature superconductors in coherent picosecond four-photon spectroscopy with high excitation level

Yu.V. Bobyrev, V.M. Petnikova, K.V. Rudenko, V.V. Shuvalov

***Abstract*. Assuming that the nonlinear response of high-temperature superconductors is caused by interband transitions in the electronic spectrum with a metastable energy gap, a model describing the results of experiments performed by picosecond coherent four-photon spectroscopy with a high excitation level is developed. It is shown that a jump in the dependence of the self-diffraction efficiency on the initial temperature of a sample should be observed in the vicinity of the point of superconducting phase transition. It is found that upon biharmonic pump – probing, the energy gap in the electronic spectrum can be detected by a specific two-photon resonance.**

Keywords: *coherent picosecond four-photon spectroscopy, high-temperature superconductors (HTSCs), high excitation level, spectral and temperature features of a HTSC nonlinear response.*

1. Introduction

Processes of rapid relaxation in high-temperature superconductors (HTSCs) are usually investigated by the pump – probe pulse method [1 – 17], which is most often used to study the dependence of the reflection (or transmission) coefficient of the excited sample on the delay time τ of the probe pulse with respect to the pump pulse [1 – 5]. It is assumed [18 – 20] that due to electron – electron (e – e) scattering, the distribution of 'hot' carriers over the energy E_e first rapidly ($\tau_{th} < 10$ fs for $E_e \sim 1$ eV [21, 22]) returns to the Fermi – Dirac distribution with the electron temperature T_e, which differs both from the initial temperature T_0 and the lattice temperature T_p [23]. Then, the temperatures of the electron and phonon subsystems are equalised ($T_e \to T_p$) for the time τ_R due to electron – phonon (e – p) scattering. Experiments have shown [1, 13, 24 – 26] that, in accordance with the theory [27 – 30], the values of τ_{th} and τ_R drastically increase in the vicinity of the superconducting transition point $T_0 \simeq T_c$. However, it was found soon [17] that such an increase is observed only at high excitation levels, when a sample should 'forget' almost immediately information on its initial state (initial temperature T_0).

In [31, 32], spectral and temporal anomalies of the nonlinear-response kinetics of HTSCs pumped by high-power femtosecond pulses were interpreted within the framework of a model assuming that the energy gap in the electronic spectrum of a HTSC cannot be rapidly destroyed even when T_e strongly differs from T_p [33] and that the HTSC nonlinear response is caused by interband electronic transitions [34]. It was shown that under typical experimental conditions, the Fermi levels $E_{e,h}^F$ for free electrons (states above the energy gap) and holes (states below the energy gap) draw apart (degeneracy) and the energy difference $E_e^F - E_h^F$ drastically increases. Because processes of nonradiative three-body recombination are suppressed with increasing the energy of carriers [35], the formation of the energy gap $\Delta(T_0, T_c) \neq 0$ at $T_0 \leqslant T_c$ in the HTSC electronic spectrum drastically changes kinetics $E_e^F(t)$ and $T_{e,p}(t)$, which allows one to explain anomalies observed in the experiments.

It was shown in [36] that these anomalies should also have analogues when two picosecond pulses coincident in time are used to excite a HTSC and probe its states by variations in the reflection and transmission coefficients. In this case, the degeneracy (separation of the Fermi levels $E_{e,h}^F$) should be manifested in a nontrivial dependence of the HTSC nonlinear response on the initial temperature (sharp jump in the vicinity of the point $T_0 \simeq T_c$).

Below, by using the calculated kinetics $E_e^F(t)$ and $T_{e,p}(t)$ [36], we will show that, when two other methods of picosecond nonlinear spectroscopy (biharmonic pumping [8] and degenerate four-photon spectroscopy [37]) are used, similar jumps should be observed in the vicinity of the point $T_0 \simeq T_c$ in the dependence of the HTSC nonlinear response on the initial temperature T_0. In this case, the energy gap in the electronic spectrum of the HTSC upon biharmonic pumping can be also detected by a specific two-photon resonance [8, 38].

2. Nonlinear response model

Thus, we consider here the stationary (picosecond) version of the methods of biharmonic pumping (BP) [8] and degenerate four-photon spectroscopy (DFPS) [37]. We will assume that a sample is excited and probed by two comparatively long 20-ps pulses at wavelengths $\lambda_{1,2}$ (frequencies $\omega_{1,2}$), which coincide in time but propagate at an angle to each other (the wave vectors $\boldsymbol{k}_1 \neq \boldsymbol{k}_2$). The parameter being measured is the dependence of the self-

Yu.V. Bobyrev, V.M. Petnikova, K.V. Rudenko, V.V. Shuvalov
International Laser Center, M.V. Lomonosov Moscow State University, Vorob'evy gory, 119992 Moscow, Russia;
e-mail: vsh@vsh.phys.msu.ru

Received 20 March 2006
Kvantovaya Elektronika **36** (5) 408 – 414 (2006)
Translated by M.N. Sapozhnikov

diffraction efficiency η (the efficiency of the field generation in the direction $\boldsymbol{k}_3 = 2\boldsymbol{k}_1 - \boldsymbol{k}_2$ at the frequency $\omega_3 = 2\omega_1 - \omega_2$) on the frequency detuning $\Delta\omega = \omega_1 - \omega_2$ of pump components (the BP method [8]) or on the excitation–probe wavelength λ when the frequencies of these components coincide ($\omega_1 = \omega_2$) (DFPS [37]).

The self-diffraction process was described by using the model of coherent four-photon response developed in [39]. It was assumed that the total cubic nonlinear susceptibility χ of a sample consists of a few components:

$$\chi = \chi_r + \chi_{nr} + \chi_s + \chi_0. \quad (1)$$

Here, χ_r and χ_{nr} are the resonance and nonresonance (see below) parts of the electronic response, respectively, caused by interband transitions; χ_s is the nonlinear susceptibility component related to the scattering of electrons by acoustic phonons; and χ_0 is a constant related to some errors of the model, first of all, to a finite size of the integration region over the initial and final electronic states. The restriction of this region in numerical calculations (see below) inevitably introduces errors in the description of nonresonance processes caused by transitions to neglected bands, absorption by free carriers, etc.

We calculated χ_{nr} by the method [39], which we already used earlier. This method takes into account in a standard way [40] the contributions from all possible one- and two-photon resonance electronic transitions in the real electronic spectrum of the HTSC sample (calculated from the data taken from the literature [41]) and their real occupation numbers (calculated from the kinetic data for E_e^F and $T_{e,p}$ [36]):

$$\chi_{nr} \propto P_0[K_+P_+ + K_-P_-], \quad (2)$$

where

$$P_0 = \sum_{i,i'} \int\int \frac{|d_{i,i'}(\boldsymbol{k},\boldsymbol{k}')|^2 n_i(\boldsymbol{k})[1 - n_{i'}(\boldsymbol{k}')]}{[\omega_1 - \Omega_{i,i'}(\boldsymbol{k},\boldsymbol{k}') - i\Gamma_{i,i'}(\boldsymbol{k},\boldsymbol{k}')]^2} d\boldsymbol{k}d\boldsymbol{k}', \quad (3)$$

$$P_\pm = \sum_{i,i'} \int\int \frac{|d_{i,i'}(\boldsymbol{k},\boldsymbol{k}')|^2 n_i(\boldsymbol{k})[1 - n_{i'}(\boldsymbol{k}')]}{[\omega_1 \pm \Delta\omega - \Omega_{i,i'}(\boldsymbol{k},\boldsymbol{k}') \pm i\Gamma_{i,i'}(\boldsymbol{k},\boldsymbol{k}')]^2} d\boldsymbol{k}d\boldsymbol{k}', \quad (4)$$

$$K_\pm = \sum_{i,i'} \int\int \frac{|d_{i,i'}(\boldsymbol{k},\boldsymbol{k}')|^2 n_i(\boldsymbol{k})[1 - n_{i'}(\boldsymbol{k}')]}{[\pm\Delta\omega + \Omega_{i,i'}(\boldsymbol{k},\boldsymbol{k}') \pm i\Gamma_{i,i'}(\boldsymbol{k},\boldsymbol{k}')]} d\boldsymbol{k}d\boldsymbol{k}'. \quad (5)$$

Here, i and i' numerate the bands involved in the $(i,\boldsymbol{k}) \to (i',\boldsymbol{k}')$ electronic transition with the dipole moment $d_{i,i'}(\boldsymbol{k},\boldsymbol{k}')$ and the resonance frequency $\Omega_{i,i'}(\boldsymbol{k},\boldsymbol{k}') = E_{i'}(\boldsymbol{k}') - E_i(\boldsymbol{k})$; $\boldsymbol{k}$ is the electron quasi-momentum; $E_i(\boldsymbol{k})$ and $n_i(\boldsymbol{k})$ are the normalised energy and the occupation number of the $(i,\boldsymbol{k})$ state, respectively; and $\Gamma_{i,i'}(\boldsymbol{k},\boldsymbol{k}')$ is the relaxation rate of the interband polarisation.

We calculated χ_{nr} assuming that the $(i,\boldsymbol{k}) \to (i',\boldsymbol{k}')$ transitions are always direct ($\boldsymbol{k} = \boldsymbol{k}'$), and $d_{i,i'}(\boldsymbol{k},\boldsymbol{k}') = d$ and $\Gamma_{i,i'}(\boldsymbol{k},\boldsymbol{k}') = \Gamma$ are constants independent of i, i' and $\boldsymbol{k}$. The transition frequencies $\Omega_{i,i'}(\boldsymbol{k},\boldsymbol{k}')$ were found by the interpolation of data [32, 36] on the electronic spectrum of La_2CuO_4 at room temperature [41] taking into account the requirements to the symmetry and periodicity [39]. As before [31, 32, 36], the cooling of the sample was simulated by the replacement $E_i(\boldsymbol{k}) \to E_0^F \pm \{[E_i(\boldsymbol{k}) - E_0^F]^2 + \Delta(T_0)^2\}^{1/2}$ for $E_i(\boldsymbol{k}) > E_0^F$ and $E_i(\boldsymbol{k}) < E_0^F$, respectively, which described the redistribution of the density of states near the Fermi surface during the phase transition. The energy gap

$$\Delta(T_0) \equiv \begin{cases} 3.12k_B T_c(1 - T_0/T_c)^{1/2} & \text{for } T_0 \leqslant T_c, \\ 0 & T_0 > T_c \end{cases} \quad (6)$$

was assumed a constant depending only on T_0 and T_c (frozen gap [33] of the s symmetry in the weak coupling approximation of the BCS theory [42]). Here, E_0^F is the equilibrium (initial) position of the Fermi level and k_B is the Boltzmann constant. Integration was performed by the method of singularities over zones lying in the range $|E_i(\boldsymbol{k}) \pm E_0^F| \leqslant 2.5$ eV [43]. The occupation numbers $n_i(\boldsymbol{k})$ were assumed constants specified by the Fermi–Dirac distribution with the thermodynamic parameters $\langle E_e^F \rangle_t$ and $\langle T_e \rangle_t$ calculated in [36] and averaged over the pump pulse duration $\tau_p = 20$ ps. This simulated the situation with pump and probe pulses coincident in time in experiments with a $\sim$200-nm thick $YBa_2Cu_3O_{7-\delta}$ film (with the phase transition temperature $T_c = 91$ K) on a $SrTiO_3$ substrate absorbing 30 % of the total energy 4×10^{-7} J of the pump pulses focused into a spot of diameter 150 μm. The only fitting parameter of the model in the calculation of χ_{nr} was the relaxation rate of polarisation, whose value $\Gamma = 150$ cm^{-1} was selected to fit the width of the nonlinear response spectral features in DFPS experiments [5, 24] by the corresponding calculated width and was not varied further.

It is obvious that the approximation $\boldsymbol{k} = \boldsymbol{k}'$ that we used in the calculation of χ_{nr} leads to the loss of contributions introduced by the two-photon resonance transitions $\boldsymbol{k} \to \boldsymbol{k}'$ between the two states of the conduction band separated by the energy gap. Taking the relation $\boldsymbol{k}' = \boldsymbol{k} + \boldsymbol{k}_1 - \boldsymbol{k}_2$ into account, the role of such transitions will be substantial only for the states localised in the comparatively narrow vicinity $|\boldsymbol{k}| \leqslant |\boldsymbol{k}^F| - |\boldsymbol{k}_1 - \boldsymbol{k}_2|$ near the Fermi surface for $\Delta\omega \sim 2\Delta(T_0)$. Strictly speaking, this circumstance explains the term 'nonresonance part of the electronic nonlinear response' by which we denoted χ_{nr}.

However, because of a sharp jump in the density of states in the vicinity of the Fermi level in a HTSC, the role of such transitions can be quite important. For this reason, we introduced the additional resonance component χ_r to the total response χ, whose main function was to take the corresponding contributions into account. This component was calculated by using the model of an effective two-level system [44], i.e., we neglected the anisotropy of the band structure of a sample and performed integration in (3)–(5) over the energy E_i taking into account the condition $E_{i'} - E_i = 2\Delta(T_0)$, similarly to the approach used in [31]. As a result, the weight of the component χ_r with respect to χ_{nr} ceased to be unambiguously defined and it was treated further as a fitting parameter proportional to T_0^2 (due to the increase in the amplitude and slope of the density of states with decreasing the initial temperature) and equal to 0.5 at $T_0 = 90$ K. The value of this parameter was not varied further as well. Note that the value of χ_r was calculated by using the relaxation rate of polarisation $\Gamma = 50$ cm^{-1} at the $\boldsymbol{k} \to \boldsymbol{k}'$ transition that was much lower than that used in the calculation of χ_{nr} (see above), because only in this case the spectral features of the nonlinear response in the BP method corresponded to the real experiment [8, 9]. In principle,

there is no wonder in this circumstance because relaxation processes should be drastically slowed down near the boundaries of the bands of the allowed states [15, 21, 24].

The contribution of processes involving acoustic phonons was calculated from the expression

$$\chi_s = -\frac{\chi_{ac}}{(\Delta\omega)^2 + (4\delta\omega)^2 + i4\delta\omega\Delta\omega}, \quad (7)$$

which follows from conventional expressions for the Mandelstam–Brillouin nonlinearity [45] convoluted with the spectra of two pump components taking into account that the duration τ_p of the pump–probe pulses is short compared to the characteristic decay time of sound. The spectral width $\delta\omega = 1.5$ cm^{-1} of the pump components was strictly specified by the conditions of real experiments [8, 9]. As a result, this component of the total nonlinear response χ also contained a single fitting parameter – the complex amplitude χ_{ac} which was assumed proportional to T_0 (due to an increase in the occupation numbers of acoustic phonon modes with increasing the initial temperature).

We assumed in the numerical simulation of the nonlinear response in the BP method that both pump components have a wavelength of 650 nm at the frequency coincidence point $\Delta\omega = 0$, i.e., they are localised in the spectral region where the nonlinear response of a sample should be maximal both in experiments [5, 24] and theory [31, 32, 34]. The results of calculations were fitted only by two parameters. It was assumed that the amplitude χ_{ac} of the component χ_s and also χ_0 should be chosen so that due to interference of all the contributions into χ, the dependence of the self-diffraction efficiency $\eta(\Delta\omega, T_0) \propto |\chi(\Delta\omega, T_0)|^2$ would have 'dips' at two points $\Delta\omega = 10$ cm^{-1} at $T_0 = 90$ K and $\Delta\omega = 63$ cm^{-1} at $T_0 = 80$ K, in accordance with the experimental data [8]. Note, however, that the frequency coincidence point of the BP components chosen in [8] was different and corresponded to $\lambda \simeq 620$ nm. The dependences $\eta(\lambda, T_0) \propto |\chi(\lambda, T_0)|^2$ measured by the DFPS method were calculated already without any fitting by using the same expressions (1)–(5) and procedures taking into account the condition $\Delta\omega = 0$ and the values of χ_{ac} and χ_0 found from the criterion described above.

3. Results of simulations

Figure 1 illustrates the calculated transformation of the dependence of the nonresonance component χ_{nr} of the total nonlinear susceptibility χ of a sample on the frequency detuning $\Delta\omega$ of the pump components with changing the initial temperature T_0 of the sample. The variations of the real (Fig. 1a) and imaginary (Fig. 1b) parts of χ_{nr} are presented at the semi-logarithmic scale in the $(\Delta\omega, T_0)$ plane. One can easily see that due to the reasonable value of Γ (150 cm^{-1}, see above) selected for the calculation of this component, the obtained family of dependences $\chi_{nr}(\Delta\omega)$ has distinct spectral features. Note also that the dependence $\mathrm{Im}\,\chi_{nr}(\Delta\omega)$ is transformed most strongly with changing T_0. A characteristic jump of the component χ_{nr} in the vicinity of the phase transition point $T_0 \sim T_c$, which was early discussed for the picosecond probe pulse method [36], is also clearly observed.

The behaviour of the real and imaginary parts of the resonance component χ_r of the total nonlinear susceptibility χ shown at the same scale in the same plane in Figs 2a and 2b, respectively, proves to be much simpler. Appearing with decreasing the initial temperature T_0 of a sample at the instant of formation of the energy gap in the electronic spectrum (at the point $T_0 = T_c$), $\chi_r(\Delta\omega)$ then simply follows the increase in the energy gap width Δ. Note also that, due to a finite relaxation rate Γ (50 cm^{-1}) used in the calculation of this component, its contribution proves to be also significant for $\Delta\omega = 0$ (the case of degenerate pump components' frequencies). Therefore, the approximation of direct interband transitions used in [32, 34] in the simulation of such a situation ($\omega_1 = \omega_2$ for $\boldsymbol{k}_1 \neq \boldsymbol{k}_2$) should inevitably result in some errors.

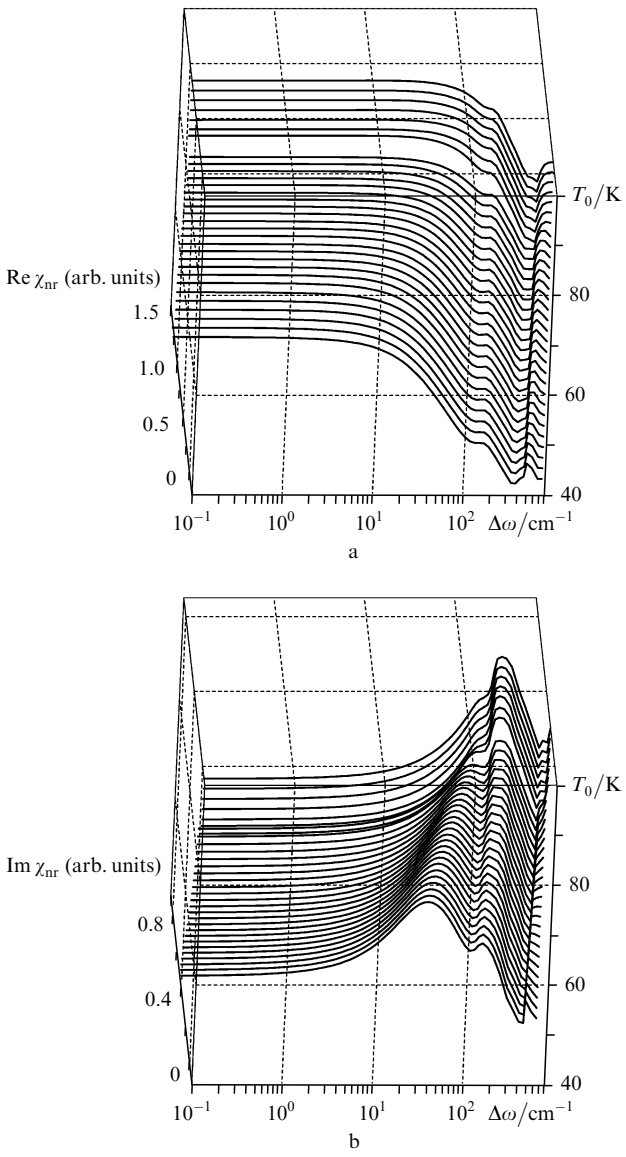

Figure 1. Variations in the real (a) and imaginary (b) parts of the nonresonance component χ_{nr} of the total nonlinear susceptibility χ in the $(\Delta\omega, T_0)$ plane (the BP method). The frequency coincidence point of the BP components $\Delta\omega = 0$ corresponds to the wavelength $\lambda = 650$ nm.

The variation in the component χ_s of the total nonlinear response χ of a sample in the $(\Delta\omega, T_0)$ plane after fitting its complex amplitude χ_{ac} according to the above criterion is illustrated in Fig. 3, where the real (Fig. 3a) and imaginary (Fig. 3b) parts are shown at the same scale. Recall that all the spectral features of this component are unambiguously

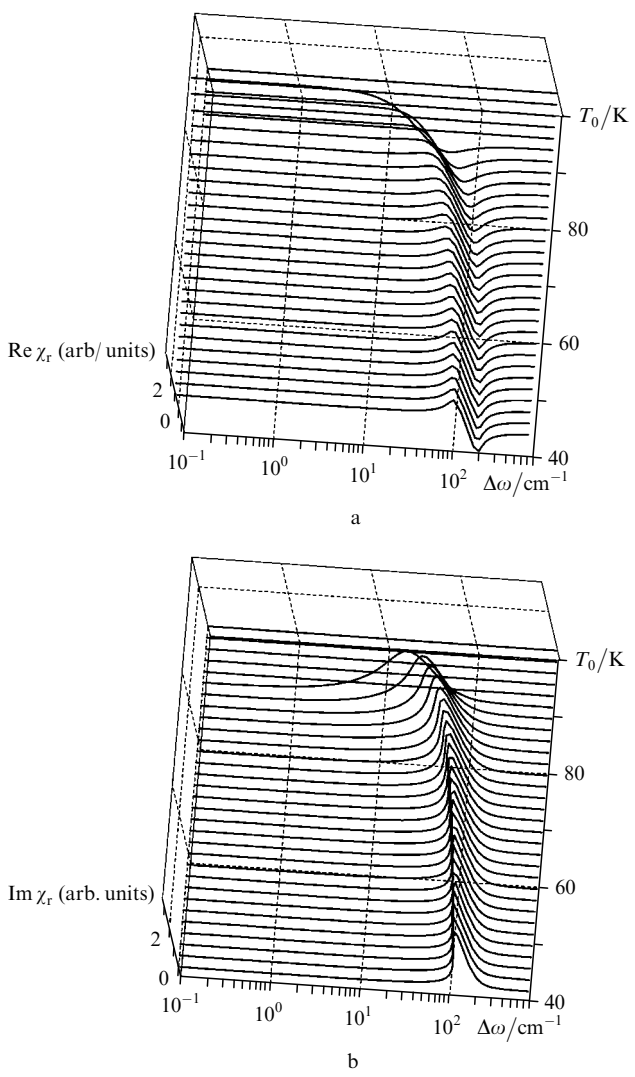

Figure 2. Variations in the real (a) and imaginary (b) parts of the resonance component χ_r of the total nonlinear susceptibility χ in the $(\Delta\omega, T_0)$ plane. The point $\Delta\omega = 0$ corresponds to $\lambda = 650$ nm.

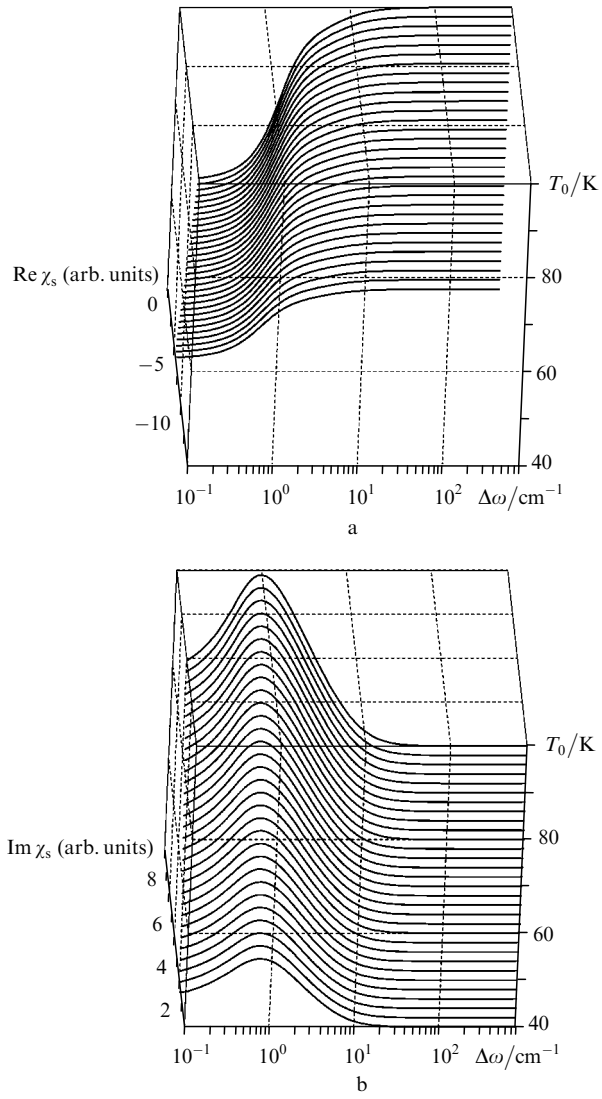

Figure 3. Variations in the real (a) and imaginary (b) parts of the component χ_s of the total nonlinear susceptibility χ in the $(\Delta\omega, T_0)$ plane (the BP method). The point $\Delta\omega = 0$ corresponds to $\lambda = 650$ nm.

determined by the pump-pulse spectral width $\delta\omega$, while the temperature properties are determined by the model itself (see above).

Figure 4 shows the dependences of the real (Fig. 4a) and imaginary (Fig. 4b) parts of the total nonlinear susceptibility χ of a HTSC sample on T_0 and $\Delta\omega$. One can easily see that the calculated dependence $\chi(\Delta\omega, T_0)$ preserves all the features of its components considered above. This is illustrated even more clearly in Fig. 5, which presents both real experimental data (Fig. 5a) [8] and the calculated dependence $\eta(\Delta\omega, T_0) \propto |\chi(\Delta\omega, T_0)|^2$ (Fig. 5b) in approximately the same detuning range Δ of the BP components and the same range of the initial temperatures T_0 of a HTSC sample plotted at the double logarithmic scale. Taking into account the use of only two fitting parameters in such a complicated model, the different frequency coincidence points of the BP components and experimental errors, the agreement obtained for the whole family of experimental and theoretical dependences appears quite satisfactory.

Figure 6 illustrates the transformation of the dependences of the real (Fig. 6a) and imaginary (Fig. 6b) parts of the nonresonance component χ_{nr} of the total nonlinear susceptibility χ of the HTSC sample on the pump wavelength λ with changing the initial temperature T_0 in the case of degenerate frequencies ($\Delta\omega = 0$ in the DFPS method). One can easily see that the consideration of the real band structure of the sample gives rise to distinct spectral features in the dependence $\chi_{nr}(\lambda)$, which weakly depend on the initial temperature T_0 and agree as a whole with experiments [5, 24] and calculations [31, 32, 34] for the probe pulse method. A characteristic jump in the χ_{nr} value in the vicinity of the phase transition point $T_0 \sim T_c$ is also distinctly observed.

Figure 7 shows variations in the real part of the resonance component $\text{Re}\,\chi_r$ (Fig. 7a) of the total nonlinear response χ and the modulus of the latter $|\chi|$ (Fig. 7b) in the same (λ, T_0) plane. The dependence of the imaginary part $\text{Im}\,\chi_r(\lambda, T_0)$ is not presented here because its value is almost two orders of magnitude smaller than the real part. The components χ_s and χ_0 are also not shown because their value within the framework of the model for $\Delta\omega = 0$ is independent of the pump–probe wavelength. It follows from Fig. 7b that the dependence of the self-diffraction efficiency $\eta(\lambda, T_0) \propto |\chi(\lambda, T_0)|^2$ measured by the DFPS

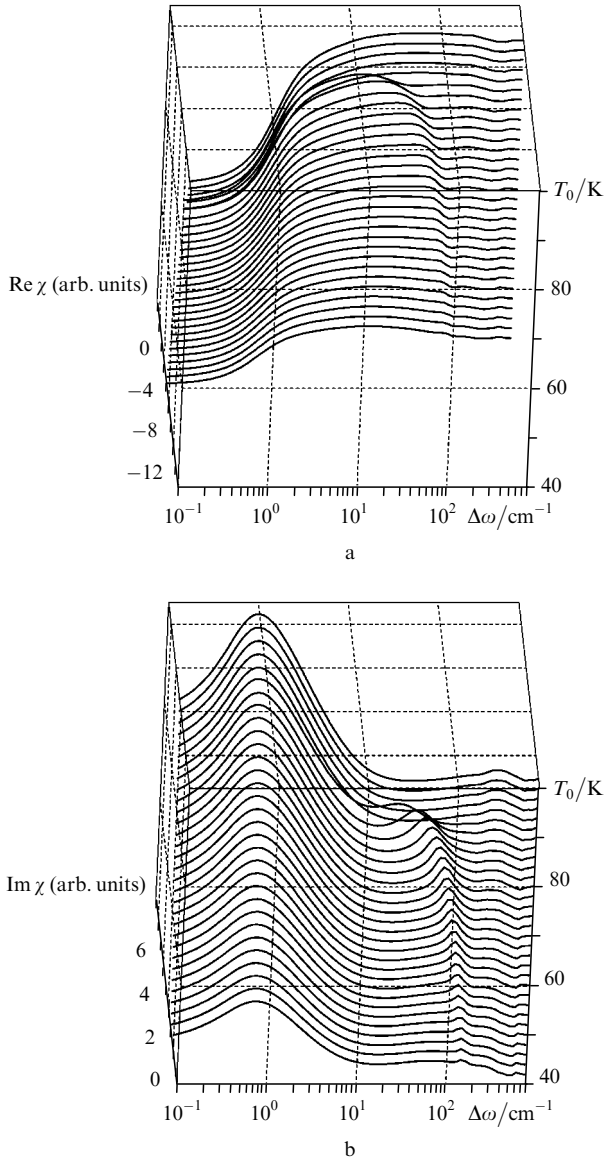

Figure 4. Variations in the real (a) and imaginary (b) parts of the total nonlinear susceptibility χ in the $(\Delta\omega, T_0)$ plane (the BP method). The point $\Delta\omega = 0$ corresponds to $\lambda = 650$ nm.

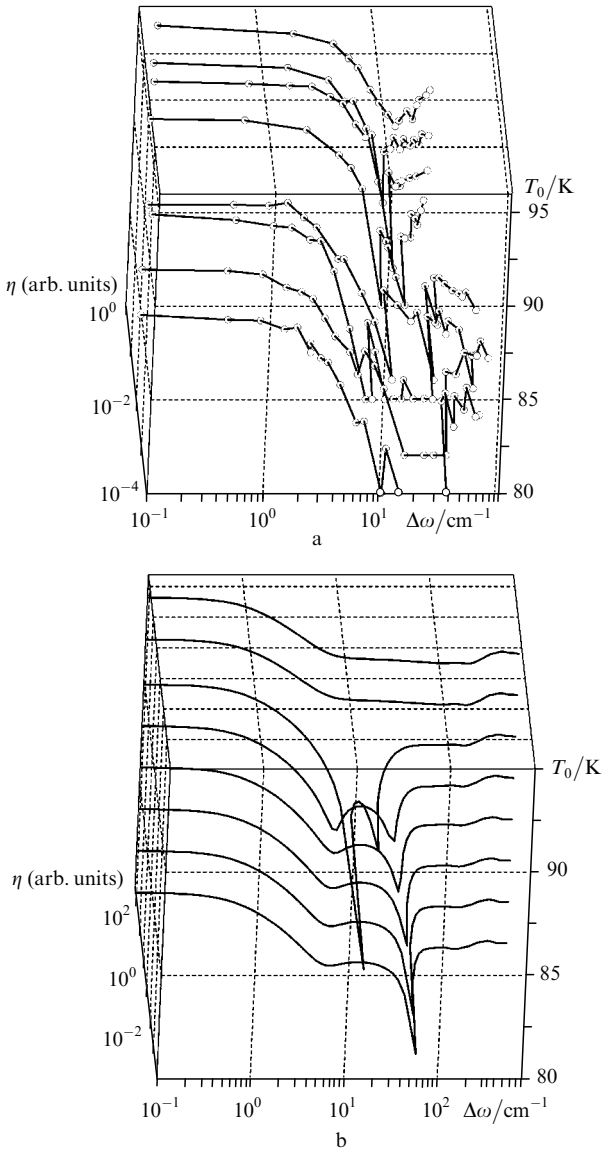

Figure 5. Experimental [8] (a) and calculated (b) dependences $\eta(\Delta\omega, T_0)$ (the BP method). The point $\Delta\omega = 0$ corresponds to wavelengths $\lambda = 620$ (a) and 650 nm (b).

method also preserves the above-mentioned features of the components of χ. First, this dependence has distinct maxima and minima, whose spectral position relatively weakly depends on the initial temperature T_0. Second, a sharp jump in the self-diffraction efficiency is observed in the vicinity of the phase transition point $T_0 \sim T_c$. Thus, spectral and temporal features of $\eta(\lambda, T_0)$ observed by this method prove to be similar to those of the nonlinear response in the pump-probe pulse method described in [31, 32, 34, 36].

4. Conclusions

By assuming that the energy gap in the electronic spectrum of a HTSC is metastable [9, 31–34, 36] and its nonlinear response is caused by interband electronic transitions [5, 24, 31, 32, 34, 36], we have simulated the results of experiments on picosecond coherent four-photon spectroscopy of HTSCs (methods of biharmonic pumping [8, 9] and degenerate four-photon spectroscopy [37]). It has been shown that under typical experimental conditions at sufficiently high excitation levels (the pump pulse energy $\sim 10^{-7}$ J in a spot of diameter 150 μm), sharp jumps should be observed in the vicinity of the superconducting transition point $T_0 \simeq T_c$ in the dependence of the self-diffraction efficiency on the initial temperature T_0 of a sample. Despite strong heating, the energy gap in the electronic spectrum of a HTSC can be found by the BP method in this case as well by the presence of a two-photon resonance [8, 38], which can explain the results obtained in [9].

However, it is even more important, in our opinion, that the model developed in [31, 32, 34] and here can explain almost all the temperature, spectral, and temporal anomalies in the behaviour of the nonlinear response of HTSCs observed earlier by various methods of nonlinear spectroscopy. Such anomalies have been always observed in many experiments performed by the methods of pump-probe pulse, biharmonic pumping, and degenerate four-photon spectroscopy at different excitation levels by using femto-

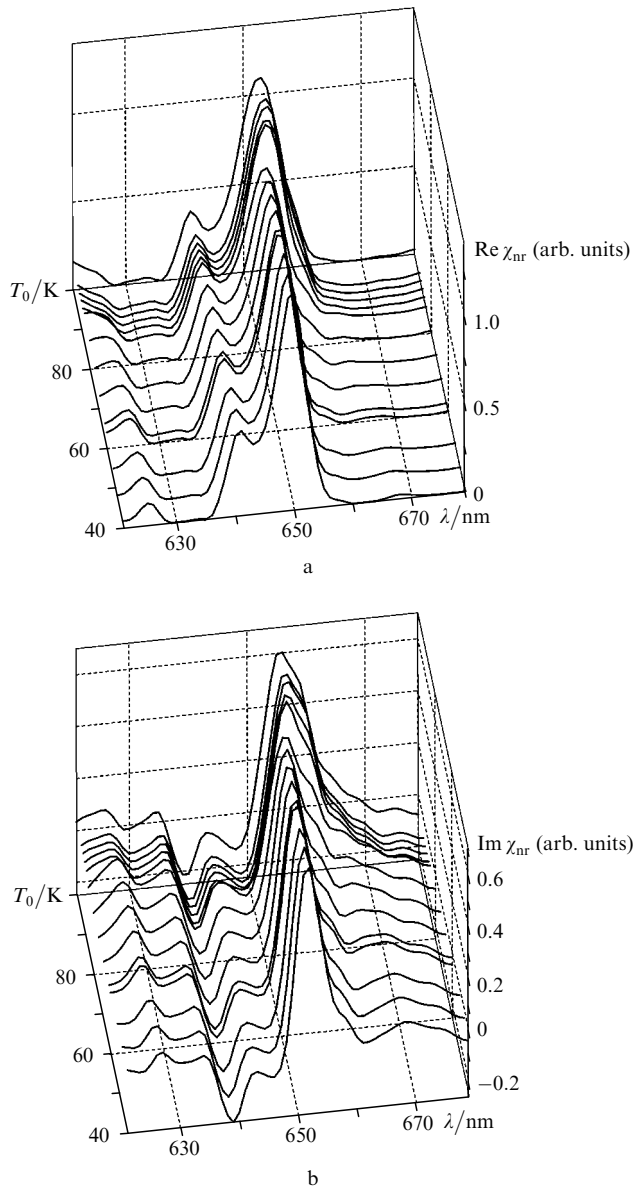

Figure 6. Variations in the real (a) and imaginary (b) parts of the nonresonance component χ_{nr} of the total nonlinear susceptibility χ in the (λ, T_0) plane (the DFPS method).

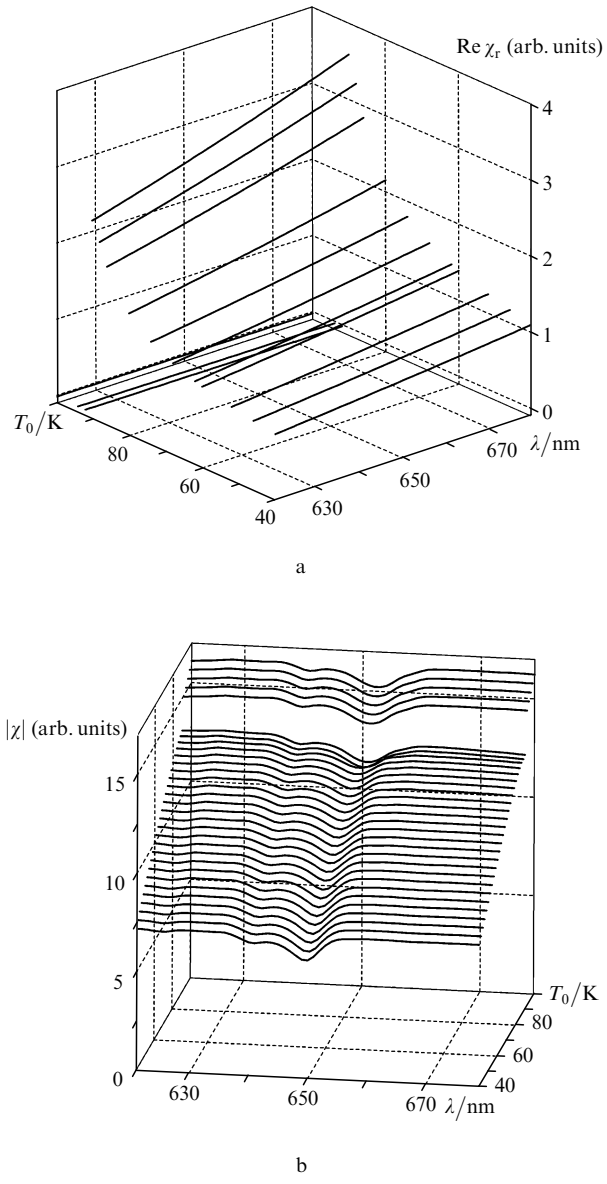

Figure 7. Variations in the real part (a) of the resonance component Re χ_r of the total nonlinear susceptibility χ and the modulus $|\chi|$ (b) in the (λ, T_0) plane (the DFPS method).

second and picosecond pulses. Up to the present, the models used to interpret such anomalies could explain the results of only one particular experiment and contradicted to other known experimental data.

Acknowledgements. This work was supported by Grants No. NSh-1583.2003.2 and No. MK-1328.2004.2 of the President of the Russian Federation.

References

1. Han S.G. et al. *Phys. Rev. Lett.*, **65**, 2708 (1990).
2. Brorson S.D. et al. *Phys. Rev. Lett.*, **64**, 2172 (1990).
3. Gershenzon M.E. et al. *Pis'ma Zh. Eksp. Teor. Fiz.*, **52**, 1189 (1990).
4. Kazeroonian A.S. et al. *Sol. State Commun.*, **78**, 95 (1991).
5. Chekalin S.V. et al. *Phys. Rev. Lett.*, **67**, 3860 (1991).
6. Bluzer N. *Phys. Rev. B*, **44**, 10222 (1991).
7. Hegman F.A. et al. *Appl. Phys. Lett.*, **62**, 1158 (1993).
8. Zherikhin A.N. et al. *Phys. Lett. A*, **179**, 145 (1993).
9. Zherikhin A.N. et al. *Physica C*, **221**, 311 (1994).
10. Brorson S.D. et al. *Phys. Rev. B*, **49**, 6185 (1994).
11. Buhleier R. et al. *Phys. Rev. B*, **50**, 9672 (1994).
12. White J.O. et al. *Physica C*, **235–240**, 2025 (1994).
13. Stevens C.J. et al. *Phys. Rev. Lett.*, **78**, 2212 (1997).
14. Smith D.C. et al. *J. Low Temp. Phys.*, **117**, 1059 (1999).
15. Demsar J. et al. *Phys. Rev. B*, **63**, 054519 (2001).
16. Segre G.P. et al. *Phys. Rev. Lett.*, **88**, 137001 (2002).
17. Schneider M.L. et al. *Europ. Phys. J. B*, **36**, 327 (2003).
18. Owen C.S., Scalapino D.J. *Phys. Rev. Lett.*, **28**, 1559 (1972).
19. Parker W.H., Williams W.D. *Phys. Rev. Lett.*, **29**, 924 (1972).
20. Schuller I., Gray K.E. *Phys. Rev. Lett.*, **36**, 429 (1976).
21. Allen P.B. *Phys. Rev. Lett.*, **59**, 1460 (1987).
22. Nessler W. et al. *Phys. Rev. Lett.*, **81**, 4480 (1998).
23. Sun C.K. et al. *Phys. Rev. B*, **50**, 15337 (1994).
24. Farztdinov V.M. et al. *Brazilian J. of Physics*, **26**, 482 (1996).
25. Demsar J. et al. *Phys. Rev. Lett.*, **82**, 4918 (1999).
26. Kabanov V.V. et al. *Phys. Rev. B*, **61**, 1477 (2000).
27. Lucas G., Stephen M.J. *Phys. Rev.*, **154**, 349 (1967).

28. Woo J.W.F., Abrahams E. *Phys. Rev.*, **169**, 407 (1968).
29. Tinkham M., Clarke J. *Phys. Rev. Lett.*, **28**, 1366 (1972).
30. Schmid A., Schoen G. *J. Low Temp. Phys.*, **20**, 207 (1975).
31. Bobyrev Yu.V. et al. *Kvantovaya Elektron.*, **35**, 720 (2005) [*Quantum Electron.*, **35**, 720 (2005)].
32. Bobyrev Yu.V. et al. *Kvantovaya Elektron.*, **35**, 729 (2005) [*Quantum Electron.*, **35**, 729 (2005)].
33. Voronov A.V. et al. *Zh. Eksp. Teor. Fiz.*, **120**, 1256 (2001).
34. Bobyrev Yu.V. et al. *Kvantovaya Elektron.*, **35**, 102 (2005) [*Quantum Electron.*, **35**, 102 (2005)].
35. Abakumov V.N. et al. *Bezyzluchatel'naya rekombinatsiya v poluprovodnikakh* (Nonradiative Recombination in Semiconductors) (St. Petersburg: B.P. Konstantinov Petersburg Institute of Nuclear Physics, RAS, 1997).
36. Bobyrev Yu.V. et al. *Kvantovaya Elektron.*, **35**, 1039 (2005) [*Quantum Electron.*, **35**, 1039 (2005)].
37. Bobyrev Yu.V. et al. *Kvantovaya Elektron.*, **32**, 789 (2002) [*Quantum Electron.*, **32**, 789 (2002)].
38. Grishanin B.A. et al. *Laser Phys.*, **3**, 121 (1993).
39. Kornienko A.G. et al. *J. Appl. Phys.*, **80**, 2396 (1996); Petnikova V.M. et al. *Kvantovaya Elektron.*, **28**, 69 (1999) [*Quantum Electron.*, **29**, 626 (1999)].
40. Schubert M., Wilhelmi B. *Nonlinear Optics and Quantum Electronics* (New York: Wiley, 1986).
41. Perry J.K. et al. *Phys. Rev. B*, **63**, 144501 (2001).
42. Lifshits E.M., Pitaevskii L.P. *Statistical Physics. Part. 2. Theory of Condensed Matter* (London: Pergamon Press, 1980; Moscow: Nauka, 1978).
43. Chadi D.J., Cohen M.L. *Phys. Rev. B*, **8**, 5747 (1973).
44. Apanasevich P.A. *Osnovy vzaimodeistviya sveta s veshchestvom* (Fundamentals of the Interaction of Light with Matter) (Minsk: Nauka i Tekhnika, 1977).
45. Akhmanov S.A., Koroteev N.I. *Metody nelineinoi optiki v spektroskopii rasseyaniya sveta* (Methods of Nonlinear Optics in Light Scattering Spectroscopy) (Moscow: Nauka, 1981).